High-Temperature Materials

SCIEPublish

Article

Enhancement on Properties of MgO-MgAlON Composite Refractories by Introducing Solid Waste Containing BN and AlN

Zhangyan Zhou [1], Lulu Wang [1,2,3], Chunming Liu [2], Chang Su [4], Huawei Yin [5], Chuanbo Hu [5], Yongxin Wang [1], Shuli Sun [6], Xinming Ren [6], Guangming Li [7], Chengcheng Zhang [7], Yongli Liu [8], Chengji Deng [9], Beiyue Ma [1,9,*] and Chao Yu [9,*]

[1] Key Laboratory for Ecological Metallurgy of Multimetallic Mineral (Ministry of Education), School of Metallurgy, Northeastern University, Shenyang 110819, China; zzy1109812710@163.com (Z.Z.); wanglljy@126.com (L.W.); wangyongxin@mails.neu.edu.cn (Y.W.)

[2] School of Materials Science and Engineering, Northeastern University, Shenyang 110819, China; cmliu@mail.neu.edu.cn (C.L.)

[3] College of Electrical Engineering, North China University of Water Resources and Electric Power, Zhengzhou 464200, China

[4] School of Metallurgy and Power Engineering, Chongqing University of Science and Technology, Chongqing 401331, China; 13322457530@163.com (C.S.)

[5] Key Laboratory of Water Environment Evolution and Pollution Control in Three Gorges Reservoir, School of Environmental and Chemical Engineering, Chongqing Sanxia University of Science and Technology, Chongqing 404100, China; huaweiyin@aliyun.com (H.Y.); huchuanbo@126.com (C.H.)

[6] Inner Mongolia Metal Material Research Institute, Yantai 264003, China; sunsl1124@outlook.com (S.S.); renxm1124@163.com (X.R.)

[7] Dashiqiao Meir Magnesium Products Co., Ltd., Yingkou 115199, China; lgm@meir.hk (G.L.); zcc@meir.hk (C.Z.)

[8] Liaoning Sidate Magnesium Industry Co., Ltd., Fushun 113122, China; liuyongli@lnsdtmy.com (Y.L.)

[9] State Key Laboratory of Advanced Refractories, Wuhan University of Science and Technology, Wuhan 430081, China; cjdeng@wust.edu.cn (C.D.)

* Corresponding author. E-mail: maceramic@126.com (B.M.); chaoyu@wust.edu.cn (C.Y.)

Received: 1 July 2026; Revised: 17 July 2026; Accepted: 24 July 2026; Available online: 6 August 2026

ABSTRACT: Driven by the goals of carbon peaking and carbon neutrality, the resource utilization of solid waste has attracted considerable attention due to its scientific importance and environmental benefits. For this purpose, MgO-MgAlON-BN refractories with enhanced thermal shock and slag resistance were designed and successfully fabricated by introducing BN solid waste as an additive. The results indicate that the sample containing BN additives exhibits superior overall performance compared with those without additives. At a BN content of 3.26 wt.%, the cold compressive strength increases by 21.20%, and the contact angle at 1723 K increases by 50.01%. Further analysis reveals that the improved wetting behavior is mainly attributed to the introduction of BN additives, which promote the formation of numerous micro-convex structures. These structural characteristics restrict slag infiltration and inhibit slag penetration into the refractory matrix, thereby enhancing slag resistance. Consequently, a cost-effective and feasible reinforcement strategy for MgO-MgAlON-BN refractories is proposed, providing a promising pathway for the high-value utilization of solid waste resources.

Keywords: MgO-MgAlON-BN composite refractories; Solid waste; Apparent porosity; Strength; Slag resistance

1. Introduction

With the rapid advancement of the iron and steel industry, the accelerating transition toward low-carbon steel production has placed unprecedented demands on the refractories utilized in steelmaking processes [1–3]. Consequently, the development of low-carbon refractories has become essential to enhance both refining efficiency and the quality of steel products. However, merely reducing the carbon content in conventional MgO-C refractories to minimize a series of issues associated with high carbon content inevitably compromises their thermal shock resistance and slag corrosion resistance [4,5]. Two distinct factors primarily drive this performance degradation. First, a reduction in carbon content decreases thermal conductivity while increasing the elastic modulus, thereby adversely affecting the thermal shock resistance of MgO-C materials. Second, the diminished carbon content enhances the wettability of the material by molten slag and steel, thereby weakening its slag corrosion resistance and ultimately rendering it more susceptible to spalling and oxidation under high-temperature service conditions [6,7]. Moreover, even when low-carbon refractories are used to replace conventional MgO-C material, completely preventing the introduction of carbon impurities into molten steel remains challenging during the smelting of special steel. Therefore, the development of carbon-free refractories with excellent thermal shock resistance and slag corrosion resistance is of great significance for the production of high-quality special steel.

Magnesium aluminum oxynitride (MgAlON), featuring a spinel structure, exists as a solid solution within the Al_2O_3-AlN-MgO ternary system [8]. MgAlON and MgAlON-based composites have emerged as promising high-quality refractories for lining RH refining furnaces due to their excellent mechanical properties, good thermal shock resistance, low pollution of molten steel, poor wettability with slag and molten steel, and outstanding slag corrosion resistance [9–11]. However, the synthesis of MgAlON primarily relies on pure nitrides and oxides as raw materials, resulting in high production costs that limit its widespread application. In recent years, considerable research has been devoted to optimizing the synthesis of MgAlON and its composite materials. For example, Ma et al. [12] prepared MgAlON powders in a nitrogen atmosphere using MgO, γ-Al_2O_3, and carbon black as raw materials, and subsequently produced MgAlON ceramics through a two-step sintering process, achieving a Vickers hardness of 13.5 GPa and a flexural strength of 246 MPa. Consistent with these findings, Liu et al. [13] demonstrated that elevating the MgAlON mass fraction from 10% to 40% within a $MgAl_2O_4$-MgAlON composite increased its flexural strength and Vickers hardness from 206 MPa to 248 MPa and 9.5 GPa to 12.6 GPa, respectively. In general, the mechanical properties of composite refractories are closely related to their grain size. In this regard, Chen et al. [14] observed that prolonged holding times and elevated sintering temperatures promoted the complete development of the MgAlON phase, which suppressed grain-boundary impurities and induced microcracking healing, ultimately leading to a flexural strength of 63.1 MPa and a cold compressive strength of 136.7 MPa. These studies collectively confirm that MgAlON can effectively improve the thermal shock resistance of refractories. However, the effects of light-burned MgO, bauxite, and industrial solid waste BN on the properties of MgAlON composites remain largely unexplored. Therefore, the development of a method for the *in-situ* synthesis of MgAlON composite materials with excellent mechanical properties under pressureless sintering conditions has become a critical challenge in this field.

Boron nitride (BN) is a strongly covalent compound characterized by exceptional high-temperature chemical stability, robust thermal shock resistance, excellent oxidation resistance, and good machinability [15]. Consequently, incorporating BN into MgO-MgAlON systems to fabricate MgO-MgAlON-BN refractories offers a compelling strange to achieve complementary property enhancement. This synergistic combination is expected to significantly augment both the thermal shock resistance and slag corrosion resistance of the material, thereby broadening its industrial utility. In fact, MgO-MgAlON-BN refractories are expected to replace MgAlON-BN [16], Si_3N_4-BN [17], and sialon-BN [18] composites in applications such as nozzles and pipes for refining furnaces. Nevertheless, the strong covalent bonding between B and

N atoms at high temperature hinders material densification. To address this issue, researchers typically introduce micron-sized additives such as Y_2O_3 [19,20], B_2O_3 [21], and Al_2O_3 [22,23] to promote densification via transient liquid-phase sintering. To further reduce production costs and promote the resource utilization of industrial solid wastes, this study employed industrial solid waste BN as an additive to fabricate MgO-MgAlON-BN refractories with enhanced thermal shock resistance and slag corrosion resistance. The primary objective of this work was to clarify the influence of BN incorporation on the phase evolution, microstructural characteristics, and thermal shock behavior of MgO-MgAlON-BN refractories, as well as to reveal the underlying strengthening mechanisms. Furthermore, the wetting behavior between RH refining slag and MgO-MgAlON-BN composites was analyzed, and the general factors influencing slag-refractory interactions were explored. The novelty of this study lies in the use of industrial waste BN in a MgO-MgAlON refractory system, offering a feasible approach to simultaneously improving refractory performance and achieving high-value utilization of solid waste. These findings are expected to provide new insights into the development of high-performance and sustainable refractory materials.

2. Experimental Procedure

2.1. Raw Materials and Preparation

Light-burned magnesia (MgO 93.13 wt.%, SiO_2 5.14 wt.%, CaO 1.04 wt.%, Fe_2O_3 0.25 wt.%, other 0.44 wt.%; bulk material from Yingkou, China), Bauxite (Al_2O_3 85.68 wt.%, SiO_2 10.75 wt.%, Fe_2O_3 1.27 wt.%, CaO 0.15 wt.%, other 2.15 wt.%; bulk material from Henan Hengyuan New Materials Technology Co., Ltd., Zhengzhou, China), and AlN (Analytical reagent; from Shanghai Macklin Biochemical Technology Co., Ltd., Shanghai, China) were selected as the starting raw materials. Polyvinyl alcohol (PVA, Analytical reagent; from Shanghai Macklin Biochemical Technology Co., Ltd., Shanghai, China) was chosen as the binder. BN industrial solid waste (BN 89.21 wt.%, AlN 3.12 wt.%, Al_2O_3 3.81 wt.%, SiO_2 1.22 wt.%, other 2.64 wt.%; bulk material from Henan Nitrogen Boron New Material Technology Co., Ltd., Zhengzhou, China) was selected as the additive. MgO-MgAlON-BN composite refractories with varying BN waste concentration gradients (0 wt.%, 1.11 wt.%, 2.20 wt.%, 3.26 wt.%, and 4.30 wt.%) were synthesized via pressureless sintering. An appropriate proportion of light-burned MgO, bauxite, AlN powder, BN solid waste, and PVA was mixed according to the formulation listed in Table 1. The mixture was ball-milled in anhydrous ethanol using a planetary ball mill (QM-3SP4, from Nanjing Nanda instrument Co., Ltd., Nanjing, China) and stirred at 300 $r \cdot min^{-1}$ for 4 h to obtain the homogeneous mixtures. The resulting powders were then uniaxial pressed into cylindrical green bodies (φ20 mm × 20 mm) at 200 MPa for 3 min. Subsequently, the green bodies were dried in an oven at 353 K for 24 h. Finally, all samples were sintered at 1873 k for 6 h in a carbon-embedded atmosphere. The obtained samples were designated as 0BN, 1BN, 2BN, 3BN, and BSN, respectively.

Table 1. Compositions of the sample 0BN–4BN.

Sample	wt.%					
	Light-Burned MgO	Bauxite	AlN	BN Waste	PVA	Sintering Temperature/K
0BN	67.90	26.93	5.17	0	+3	1873
1BN	67.14	26.63	5.12	1.11	+3	1873
2BN	66.41	26.33	5.06	2.20	+3	1873
3BN	65.68	26.05	5.01	3.26	+3	1873
4BN	64.98	25.77	4.95	4.30	+3	1873

2.2. Characterization and Measurement Methods

X-ray diffraction technology (XRD) was used to analyze the phase composition of samples qualitatively. The instrument used was a D8 Advance manufactured by Bruker (Karlsruhe, Germany),

operating at a voltage of 40 kV and a current of 40 mA, with a scanning range of 5 to 90° and a scanning speed of 4°·min^{-1}. The microstructure of different samples was characterized by a scanning electron microscope (SEM, Hitachi S4800, from Hitachi, Ltd., Tokyo, Japan). The sintering properties (apparent porosity and bulk density) were according to the Archimedes' law and calculated according to Equations (1) and (2) [24].

$$P_a = \frac{m_3 - m_1}{m_2 - m_1} \times 100\% \quad (1)$$

$$D_b = \frac{m_1 D_L}{m_3 - m_2} \quad (2)$$

where P_a, m_1, m_2, m_3, D_b and D_L denote the apparent porosity (%) of the sample, the mass of dried samples (g), the apparent mass of saturated samples (g), the mass of saturated samples in air (g), the bulk density of the sample (g·cm^{-3}), and the density of impregnation liquid (deionized water) at experimental temperature (g·cm^{-3}), respectively [25]. A WDW-100 universal testing machine (CMT 5105, Shandong Wanchen Testing Machine Co., Ltd., Jinan, China) was employed to measure the cold compressive strength (P_c) at a loading speed of 0.5 mm·min^{-1}. To evaluate thermal shock resistance, the samples were subjected to an air-quenching procedure that involved heating to 1373 K for 30 min in an N_2 atmosphere, followed by cooling to room temperature. This process was defined as one cycle and repeated five times. Subsequently, thermal shock resistance was assessed using the residual strength ratio (τ), comparing values before and after quenching. The P_c and τ of the sample were presented by Equations (3) and (4) [26].

$$P_c = \frac{P}{A} \quad (3)$$

$$\tau = \frac{\sigma_a}{\sigma_b} \times 100\% \quad (4)$$

where P represents the maximum load sustained by the sample (N), and A denotes the corresponding loading area (mm^2). The residual strength retention ratio (τ, %) is defined as the ratio of the cold compressive strength of the quenched sample (δ_a, MPa) to that of the original sample (δ_b, MPa). The thermal conductivity was measured using an LFA 467 HyperFlash instrument (NETZSCH Group, Selb, Germany). The slag resistance of the sample was evaluated using the static crucible method under the carbon-embedded atmosphere.

In addition, the sessile drop method was employed to investigate the wettability behavior between the slag and the samples. The slag used in this study had a chemical composition of SiO_2 35.85%, CaO 47.32%, Al_2O_3 3.2%, MgO 7.2%, Cr_2O_3 2%, MnO 1.1%, and other 3.33%. Figure 1 shows the schematic diagram of the wettability test apparatus. The detailed experiment procedures are as follows: (1) The sintered sample and pre-melted slag were cut into discs (Φ15 mm × 3 mm) and cylinders (Φ3 mm × 3 mm), respectively. (2) When the furnace temperature reached 873 K, the sample and slag block were introduced into the furnace using an automatic moving arm. (3) The sample and slag were heated to 1723 K at heating rates of 283 K·min^{-1} from 298 to 1273 K and 278 K·min^{-1} from 1273 to 1723 K, followed by holding at 1723 K for 10 min. (4) Finally, the contact angle between the slag and the samples was determined using the spherical cap model.

The basicity index of the as-prepared MgO-MgAlON-BN composite refractories, calculated based on the mass ratio of [w(CaO) + w(MgO)]/[w(Al_2O_3) + w(SiO_2)], is approximately 2, categorizing them as basic refractories. The RH refining slag employed in the static crucible corrosion test has a chemical composition of SiO_2 35.85%, CaO 47.32%, Al_2O_3 3.2%, MgO 7.2%, Cr_2O_3 2%, MnO 1.1%, and other 3.33%, corresponding to a basicity (w(CaO)/w(SiO_2)) of 1.32. The relatively basicity of both the refractories and

the slag implies a limited thermodynamic driving force for severe interfacial chemical reactions, as the activities of SiO_2 and CaO are mutually constrained within the basicity CaO-MgO-SiO_2-Al_2O_3 system.

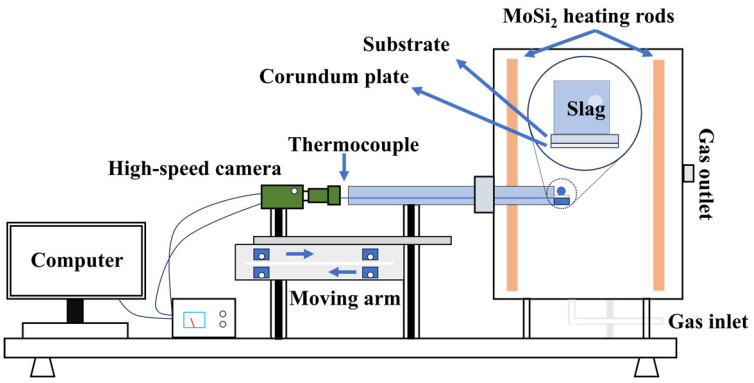

Figure 1. Schematic diagram of test instrument for slag corrosion process.

3. Results and Discussion

3.1. Phase Compositions and Microstructures

Figure 2 illustrates the XRD patterns of MgO-MgAlON-BN composite refractories with various BN solid waste additions after heat treatment at 1873 K for 6 h. MgO and MgAlON are identified as the primary crystalline phases, accompanied by minor amounts of Mg_2SiO_4 and BN. Notably, the diffraction peaks associated with $CaMgSiO_4$ disappear as the BN solid waste content increases. This phenomenon is attributed to the strong covalent bonding between B and N atoms, which enhances the viscosity of the high temperature liquid phase, thereby inhibiting the liquid phase reaction between calcium and silicon impurities [21,27]. The presence of the BN phase is further confirmed by the localized magnification of the XRD patterns, which reveals a progressive increase in peak intensity corresponding to higher BN solid waste additions. Although BN solid waste is primarily introduced as a BN source, the small amount of AlN impurity (3.12 wt.% in the waste) should also be considered during phase evolution. Based on the additional amount of BN waste (3.26 wt.% in sample 3BN), the AlN introduced from the waste accounts for approximately 0.10 wt.% of the total batch composition. This value is much lower than the amount of intentionally added AlN (5.01 wt.% in sample 3BN, as listed in Table 1). Therefore, the AlN impurity from BN waste accounts for only about 2% of the total AlN source in the system. During carbon-embedded sintering at 1873 K, AlN can participate in MgAlON formation through solid-state reactions with MgO and aluminum-containing phases (mainly derived from bauxite) [10,28]. Therefore, the additional AlN introduced by BN waste may slightly increase nitrogen availability and slightly promote MgAlON formation. However, since the amount of AlN impurity is very limited compared with the intentionally added AlN, its influence on the stoichiometry, lattice parameters, and overall phase composition of MgAlON is expected to be negligible. The phase evolution and properties of the final refractories are mainly governed by the intentionally added AlN, whereas the AlN impurity from BN waste plays only an auxiliary role and does not alter the primary reaction pathway or the conclusions of this study.

Figure 3 presents the SEM images of MgO-MgAlON-BN composite refractories with various BN solid waste additions after sintering at 1873 K for 6 h. As shown in Figure 3a, sample 1BN does not exhibit a distributed lamellar structure; instead, numerous open pores are scattered among the matrix particles (MgO and MgAlON). These pores primarily originate from the decomposition of $MgCO_3$ in the light-burned MgO. Due to an insufficient sintering driving force, the pores remain trapped within the microstructure. Consequently, the grain structure of sample 1BN is underdeveloped, resulting in a loose matrix and a mixed fracture mode consisting of both intergranular and transgranular failure [29,30]. With increasing BN solid waste content, the BN phase adopts a lamellar structure distribution within the matrix, creating a unique

microstructure. The synergistic effect between the BN lamellar and MgO small particles effectively enhances the apparent porosity, bulk density, and cold compressive strength. This improvement is primarily attributed to the excellent chemical compatibility and mechanical interlocking between the BN, MgO, and MgAlON phase. As the material density increases significantly, the grains become more closely bonded, leading to a transition toward predominantly transgranular fracture characteristics.

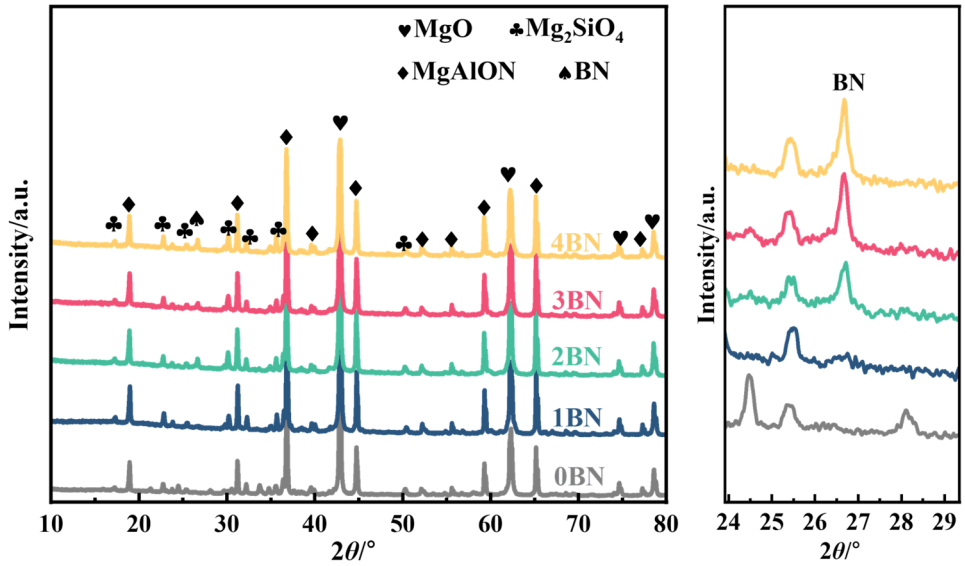

Figure 2. XRD patterns of as-sintered MgO-MgAlON refractories with various BN solid waste additions.

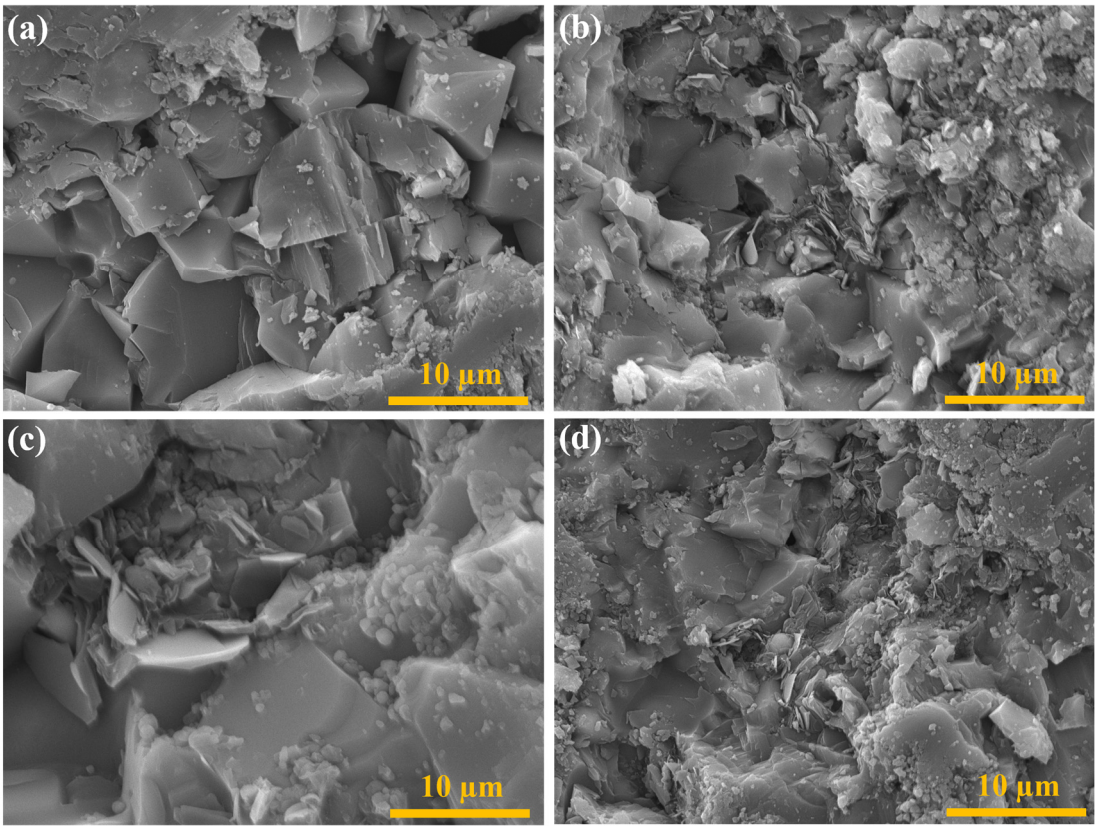

Figure 3. SEM images of the samples with various BN solid waste additions: (**a**) 1BN; (**b**) 2BN; (**c**) 3BN; (**d**) 4BN.

3.2. Apparent Porosity, Bulk Density, Thermal Shock Resistance, and Thermal Conductivity

Figure 4a shows the apparent porosity and bulk density of MgO-MgAlON-BN composite refractories with various BN solid waste additions after carbon-embedded sintering at 1873 K. Compared to the sample 0BN (apparent porosity of 13.88% and bulk density of 2.97 $g \cdot cm^{-3}$), all BN-containing specimens exhibit enhanced physical properties to varying degrees. As the BN solid waste content increases, the apparent porosity first decreases and then increases. Specifically, when the BN solid waste addition increases from 1.11 wt.% to 2.20 wt%, the apparent porosity declines from 13.25% to 12.49%, while the bulk density rises from 2.98 $g \cdot cm^{-3}$ to 3.00 $g \cdot cm^{-3}$. The sample reaches a minimum porosity of 10.29% and a corresponding maximum bulk density at a 3.26 wt.% BN. This improvement is primarily attributed to the role of BN solid waste as a sintering additive, which facilitates grain rearrangement and improves particle packing, thereby promoting densification and pore elimination [31,32]. The fine BN particles may help fill interparticle voids and promote a more homogeneous distribution of phases. In addition, BN may indirectly contribute to reaction-assisted sintering, facilitating mass transport during MgAlON formation. However, at an excessive BN content (4.30 wt.%), the bulk density decreases. As evidenced by the numerous fine particles in the cross-section (Figure 3d), redundant BN likely accumulates at the grain boundaries, thereby inhibiting grain growth [16]. In addition, BN tends to form a continuous or semi-continuous phase, which disrupts particle contact between MgAlON grains and acts as a diffusion barrier. Consequently, optimizing the BN solid waste addition is crucial for tailoring the porosity and density of MgO-MgAlON-BN composite refractories.

Figure 4b displays the evolution of the cold compressive strength of MgO-MgAlON-BN composite refractories as a function of BN solid waste addition. The cold compressive strength exhibits an inverse relationship with the apparent porosity, characterized by an initial increase followed by a subsequent decline. Specifically, the sample containing 3.26 wt.% BN (3BN) achieves a peak cold compressive strength of 308.36 MPa, after which the strength decreases slightly with further BN additions. This enhancement in mechanical performance is primarily attributed to the effects of the BN phase. On the one hand, optimal BN additions facilitate sintering densification, leading to a substantial reduction in apparent porosity. On the other hand, the lamellar BN situated at the grain boundaries induces crack deflection and branching, thereby extending the crack propagation paths and increasing the fracture energy [33]. Furthermore, the mismatch in the coefficient of thermal expansion between BN and the matrix generates interfacial residual stresses, which further reinforce the cold compressive strength of the MgO-MgAlON-BN composite refractories. These findings are corroborated by the force-displacement curves in Figure 4c, which demonstrate that the introduction of BN significantly improves the fracture energy dissipation capability (as evidenced by the larger area under the force-displacement curve) and enhances the load-bearing capacity of the MgO-MgAlON-BN composite refractories.

Figure 5 shows the cold compressive strength and the corresponding residual strength retention rate of MgO-MgAlON-BN composite refractories after five thermal shock cycles. The results indicate that the incorporation of BN solid waste enhances the thermal shock resistance of the refractories to a certain degree. Specifically, for the sample 3BN, both the residual strength retention rate and cold compressive strength reach their peak values of 65.93% and 203.31 MPa, respectively, compared to 64.21% and 163.28 MPa for the sample 0SN. However, as the BN solid waste addition exceeds 3.26 wt.%, a downward trend is observed, with the retention rate and cold compressive strength ultimately declining to 59.61% and 163.24 MPa, respectively.

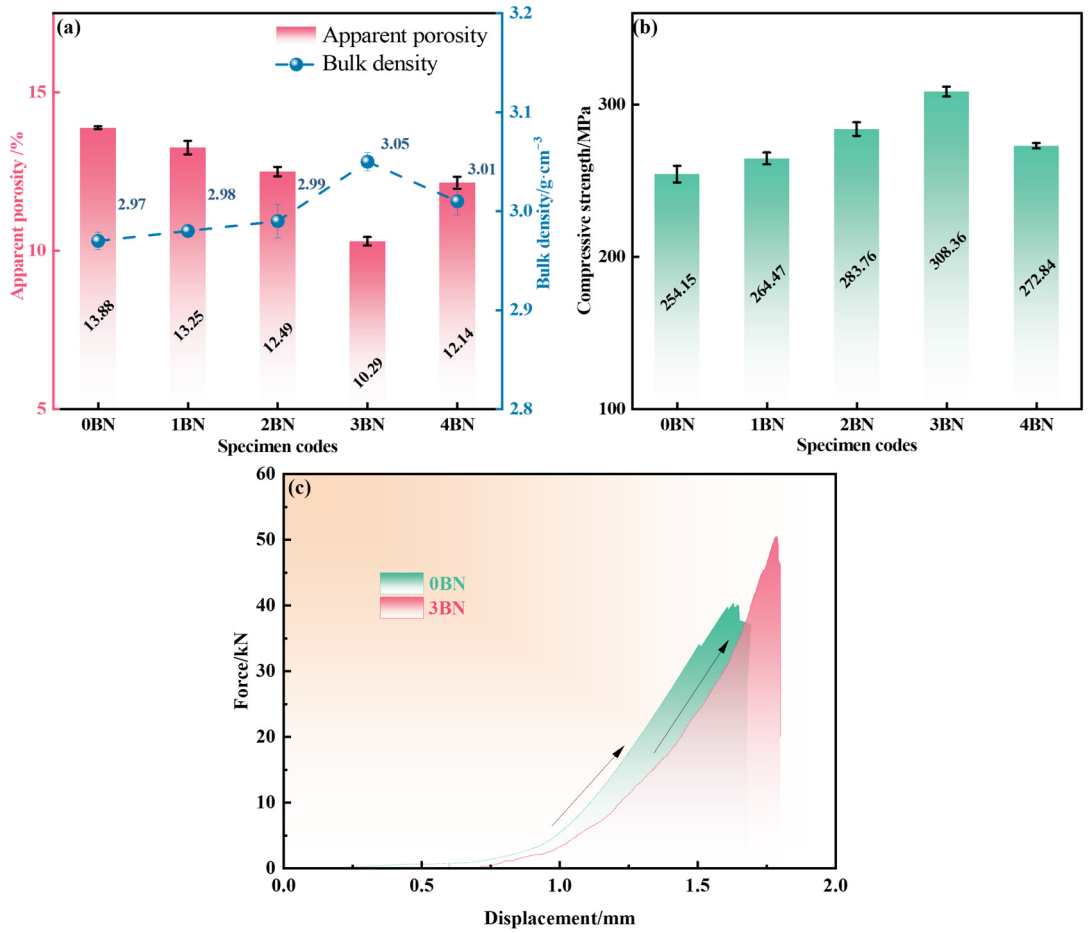

Figure 4. (**a**–**c**) Apparent porosity, bulk density, compressive strength, and force-displacement curves of MgO-MgAlON-BN refractories.

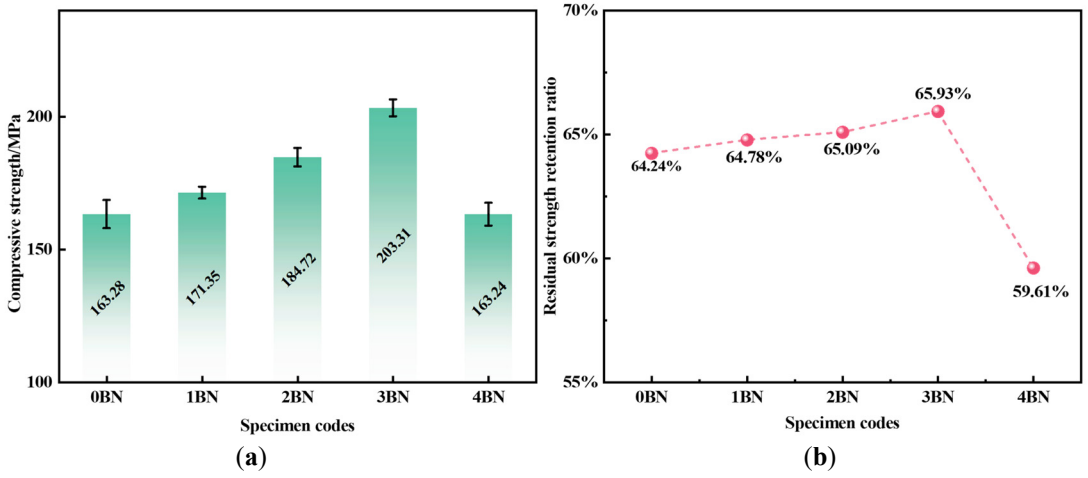

Figure 5. (**a**,**b**) The compressive strength and corresponding residual strength retention of different samples after five thermal shock cycles.

During the cooling process, the mismatch in the coefficient of thermal expansion (CTE) among the constituent phases induces significant internal stresses, which directly dictate the thermal shock resistance of the material [34]. Generally, if the second phase possesses a higher CTE than the matrix, tangential compressive and radial tensile stresses are generated during cooling [35]. Conversely, a second phase with a lower CTE has tangential tensile and radial compressive stresses. In this refractories system, BN exhibits pronounced anisotropy, with CTE values of 1×10^{-6} K^{-1} perpendicular to the hexagonal axis and 7.51 ×

10^{-6} K^{-1} parallel to it [36]. Both values are substantially lower than those of MgAlON (5.3×10^{-6} K^{-1}) and MgO (12.6×10^{-6} K^{-1}), ensuring a beneficial stress state. The existence of lamellar BN is instrumental in enhancing the thermal shock resistance of the samples. During the fracture process, an advancing crack tip encountering the BN lamellae undergoes a transition from a three-dimensional to a two-dimensional stress state. This transition promotes crack passivation and deflection, with the latter dissipating a substantial amount of fracture energy. Furthermore, the presence of BN facilitates effective grain bridging, which further elevates the fracture resistance of the MgO-MgAlON-BN composite refractories. However, excessive BN additions (e.g., sample 4BN) cause the lamellar structures to interweave and form granular aggregates, in which case the improvement of thermal shock resistance by microcracks is limited. While the incorporation of lamellar BN effectively suppresses grain boundary sliding, thereby improving the thermal shock resistance of the samples, the MgO-MgAlON-BN composite refractories cannot completely resist the fracture caused by thermal stress [36].

Figure 6 presents the thermal conductivity of MgO-MgAlON-BN composite refractories with various BN solid waste additions after heat treatment at 1873 K for 6 h. At room temperature, the thermal conductivity initially decreases from 21.19 $W \cdot m^{-1} \cdot K^{-1}$ (sample 0BN) to 18.99 $W \cdot m^{-1} \cdot K^{-1}$ (sample 1BN), followed by an increase to 24.96 $W \cdot m^{-1} \cdot K^{-1}$ (sample 2BN). A similar trend is observed at 773 K, where the values decline from 9.54 $W \cdot m^{-1} \cdot K^{-1}$ (sample 0BN) to 6.90 $W \cdot m^{-1} \cdot K^{-1}$ (sample 1BN) before recovering to 8.70 $W \cdot m^{-1} \cdot K^{-1}$ (sample 2BN). When the addition of BN solid waste was 1.11 wt.%, the presence of impurities and defects in the sample could scatter phonons, thereby shortening their mean free path and ultimately reducing the thermal conductivity [34,37]. As the BN content increases beyond 1 wt.%, the significant reduction in apparent porosity enhances the solid-phase conduction pathways, leading to the observed increase in thermal conductivity. However, the thermal conductivity of sample 4BN declines again, falling even below that of sample 0BN. This decrease is attributed to the higher apparent porosity and the aggregation of layered BN into granular clusters. These aggregated BN regions increase thermal resistance at grain boundaries and limit effective intergranular contact, thereby hindering heat transfer. Among all compositions, sample 2BN exhibits the highest thermal conductivity. However, considering the balance among thermal conductivity, slag corrosion resistance, and thermal shock resistance, sample 3BN demonstrates the most balanced overall performance. At 573 K and 773 K, the thermal conductivity of sample 3BN was 10.08% and 10.76% lower than that of sample 0BN, respectively. This indicates that the slight reduction in thermal conductivity represents an acceptable trade-off considering the significant improvements in other key properties, including cold compressive strength, slag resistance, and thermal shock resistance.

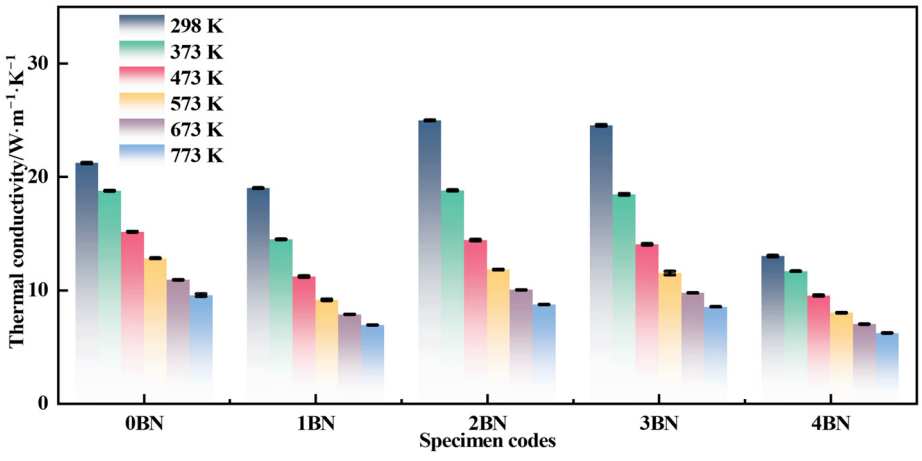

Figure 6. Thermal conductivity of MgO-MgAlON-BN refractories with different amounts of BN addition.

3.3. Analysis of Wetting Behavior

Figure 7 shows the optical images captured during the high temperature wetting process of MgO-MgAlON-BN composite refractories with various BN solid waste additions. As the temperature reaches approximately 1573 K, the slag begins to soften and assumes a hemisphere shape. With further heating, the contact angle between the slag and the sample decreases, indicating progressive slag penetration into the sample. The slag remains relatively stable in a spherical crown shape until the temperature reaches 1723 K, after which significant shape changes occur at 1723 K. To investigate the effect of BN addition on the wetting behavior, the contact angles between the slag and refractories were measured at the testing temperature. The contact angle of sample 1BN containing 1.11 wt.% BN was 34°, whereas that of sample 3BN containing 3.26 wt.% BN increased to 51°. The increased contact angle indicates reduced slag wettability, which suppresses slag spreading and infiltration into the refractory matrix, thereby improving slag resistance. In comparison, the lower contact angle of sample 1BN suggests stronger slag wettability and a greater tendency for slag penetration into the refractory pores. Therefore, the introduction of BN solid waste plays a critical role in improving the slag resistance of the MgO-MgAlON-BN composite refractories.

The basicity values of the refractory material ($R \approx 2$) and the slag ($R = 1.32$) are relatively close, indicating that the thermodynamic driving force for extensive interfacial chemical reactions is limited. According to thermodynamic principles governing slag–refractory interactions, when both phases are within the basic region of the CaO–MgO–SiO_2–Al_2O_3 system, the activities of SiO_2 and CaO remain relatively balanced, minimizing the chemical potential gradient across the interface. This reduces the driving force for the formation of low-melting phases (such as calcium silicate or aluminosilicate), which would otherwise accelerate refractory degradation. Therefore, the enhanced non-wetting behavior and suppression of slag penetration observed with increasing BN content can be attributed to the synergistic effects of physical and chemical factors. From a physical perspective, the BN-induced micro-convex surface structures restrict slag infiltration and reduce the effective solid-liquid contact area. From a chemical perspective, the favorable basicity compatibility between the refractory material and slag suppresses interfacial reactions, resulting in an increased contact angle and enhanced slag resistance with increasing BN content. In addition, the wettability results obtained at 1723 K should be regarded as a conservative evaluation of slag refractory interactions. Under actual steelmaking conditions (approximately 1873–1923 K), enhanced wetting and more intense chemical reactions may occur, thereby accelerating refractory degradation. Nevertheless, the relative performance ranking of the different BN-containing formulations (*i.e.*, sample 3BN showing superior performance among the tested samples) is expected to remain comparable at higher temperatures.

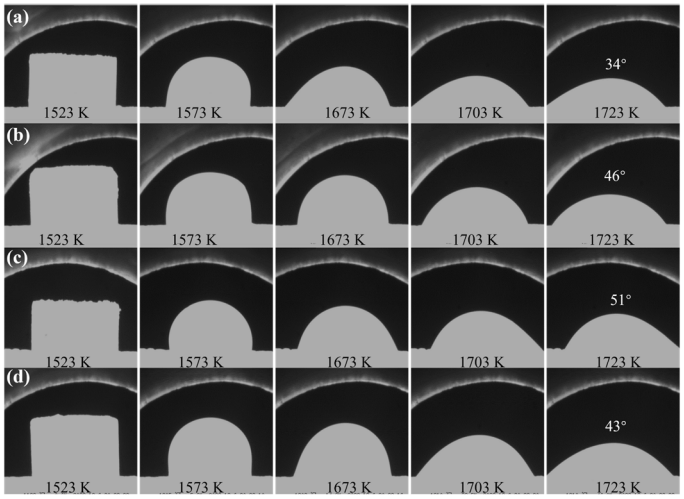

Figure 7. Wetting process of slag and MgO-MgAlON-BN refractories: (**a**) 1BN; (**b**) 2BN; (**c**) 3BN; (**d**) 4BN.

As previously established, the interaction between the molten slag and the refractories is characterized by reactive wetting, wherein the contact angle evolves as a function of time. As the interfacial chemical reaction proceeds, the interfacial tension between the slag and the refractories decreases while the adhesion strength increases [38]. These two factors directly impact the slag resistance of the material. Due to the highly similar phase compositions of the slag and refractories, achieving effective slag repellency remains a significant challenge, making it difficult to form a non-wetting contact angle exceeding 90° [39]. Hence, suppressing the inward diffusion of slag into the refractories at high temperatures becomes the primary strategy to enhance their resistance to slag corrosion. To further confirm the effect of BN solid waste addition on the wetting behavior of the sample, the surface morphologies of the samples 1BN and 3BN were characterized via SEM, as shown in Figure 8. The micrographs reveal that increasing the BN addition promotes the formation of numerous micro-convex structures on the refractory. These surface characteristics increase the surface roughness of the specimen, which restricts slag spreading and inhibits slag infiltration into the refractory matrix, thereby improving the slag resistance. As a result, slag corrosion resistance improves with increasing BN content.

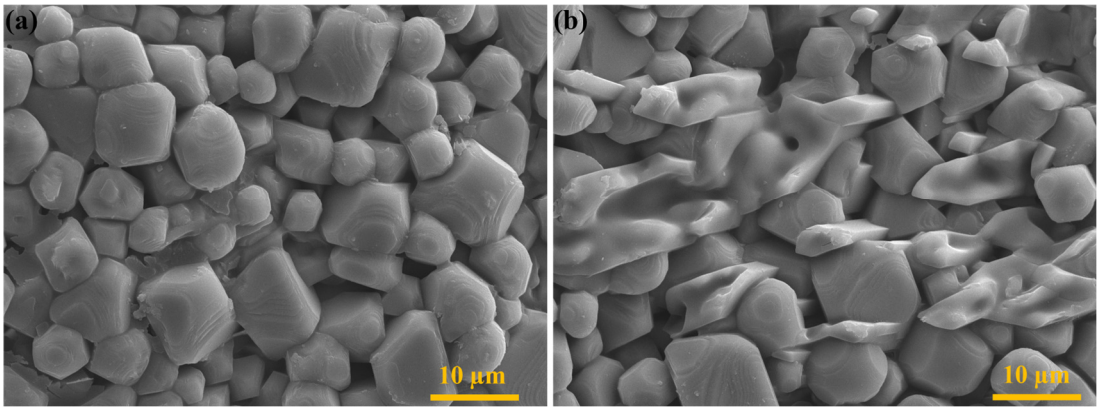

Figure 8. Surface SEM images of MgO-MgAlON-BN refractories. (**a**) 1BN, (**b**) 3BN.

4. Conclusions

In this work, a series of MgO-MgAlON-BN refractories were designed and fabricated, and the effects of BN solid waste additives and their contents on the properties of the prepared samples were investigated. The following conclusions can be drawn.

(1) An appropriate addition of BN solid waste plays a crucial role in MgO-MgAlON-BN refractories. On the one hand, it promotes sintering, effectively reducing the apparent porosity and enhancing the bulk density. On the other hand, the mismatch in thermal expansion coefficients between BN and the matrix generates residual stress at the interface, which contributes to an improvement in the cold compressive strength of the prepared samples. Moreover, increasing the BN solid waste content leads to the formation of micro-convex structures, which reduce slag penetration and thereby enhance slag resistance.

(2) With the introduction of BN solid waste, the properties of the prepared MgO-MgAlON-BN refractories have been enhanced to varying degrees. Specifically, the best performance is achieved at the addition amount of 3.26 wt.% (sample 3BN): the apparent porosity is 10.29%, the bulk density is 3.05 $g \cdot cm^{-3}$, the cold compressive strength is 308.36 MPa, the thermal conductivity is 8.09 $W \cdot m^{-1} \cdot K^{-1}$ at 773 K, the contact angle is 51° at 1723 K.

Acknowledgments

The authors gratefully acknowledge the financial support provided by the Open Project Program of State Key Laboratory of Advanced Refractories and the National Natural Science Foundation of China.

Author Contributions

Methodology, Z.Z. and L.W.; Formal Analysis, L.W., C.S., H.Y., C.H., Y.W., S.S., X.R., G.L., C.Z., Y.L., C.D. and C.Y.; Data Curation, Z.Z.; Writing—Original Draft Preparation, Z.Z.; Writing—Review & Editing, B.M.; Supervision, C.L.; Funding Acquisition, B.M. and C.Y.

Ethics Statement

Not applicable.

Informed Consent Statement

Not applicable.

Data Availability Statement

All data supporting this study are included in the article.

Funding

This research was funded by the Open Project Program of State Key Laboratory of Advanced Refractories (Grant No. SKLAR26007ZW) and the National Natural Science Foundation of China (Grant No. U20A20239).

Declaration of Competing Interest

The authors declare that they have no known competing financial interests or personal relationships that could have appeared to influence the work reported in this paper.

References

1. Yu C, Dong B, Chen YF, Ma BY, Ding J, Deng CJ, et al. Enhanced oxidation resistance of low-carbon MgO–C refractories with ternary carbides: A review. *J. Iron Steel Res. Int*. **2022**, *29*, 1052–1062. DOI:10.1007/s42243-022-00804-5
2. Fan ST, Deng CJ, Yu C, Liu ZL, Ding J. Nano-laminated BN modified graphite reinforced unfired MgO–C refractories: Preparation, properties and strengthening mechanism. *J. Mater. Res. Technol.* **2024**, *29*, 4833–4844. DOI:10.1016/j.jmrt.2024.02.201
3. Luo YX, Liu ZL, Yu C, Deng CJ, Ding J. Enhanced service performances of *in-situ* Mg-Sialon/$MgAl_2O_4$ folding structure in low carbon Al_2O_3–C refractories: Phase reconfiguration of nano-$MgSiN_2$. *J. Eur. Ceram. Soc.* **2024**, *44*, 7953–7968. DOI:10.1016/j.jeurceramsoc.2024.05.066
4. Chong XC, Li KD, Xiao GQ, Ding DH, Hou X. Effect of C/MgO nanocomposite powders on the properties of low-carbon MgO–C refractories. *Ceram. Int.* **2023**, *49*, 34316–34326. DOI:10.1016/j.ceramint.2023.08.152
5. Ren XM, Ma BY, Sun SL, Wang ZH, Ji W, Hou SY, et al. Self-reinforced and eco-friendly porous MgO-based ceramics from magnesite tailings: The effect of La_2O_3 and firing temperature. *Ceram. Int.* **2024**, *50*, 12992–13002. DOI:10.1016/j.ceramint.2024.01.209
6. Feng CZ, Xiao GQ, Ding DH, Lei CK, Lv LH, Chong XC, et al. Enhanced thermal shock resistance of low-carbon Al_2O_3-C refractories via CNTs/$MgAl_2O_4$ whiskers composite reinforcement. *J. Am. Ceram. Soc.* **2024**, *107*, 3881–3894. DOI:10.1111/jace.19673
7. Luo YX, Wang X, Liu ZL, Yu C, Deng CJ, Ding J. Enhanced oxidation resistance and thermal shock resistance of low-carbon Al_2O_3–C refractories with nano-BN: A synergistic of mullitization behavior. *J. Alloys Compd.* **2024**, *975*, 172937. DOI:10.1016/j.jallcom.2023.172937

8. Zhang RS, Wang H, Tian M, Wang YZ, Liu MY, Wang HM, et al. Pressureless reaction sintering and hot isostatic pressing of transparent MgAlON ceramic with high strength. *Ceram. Int.* **2018**, *44*, 17383–17390. DOI:10.1016/j.ceramint.2018.06.203
9. Cheng X, Liu L, Xiao LH, Huo XT, Guo M, Zhang M. Effect of MgO on corrosion mechanism under LF refining slag for MgAlON–MgO composites synthesized from spent MgO–C brick: Wetting behaviour, reaction process and infiltration mechanism. *J. Alloys Compd.* **2023**, *963*, 171278. DOI:10.1016/j.jallcom.2023.171278
10. Wang LL, Zhou ZY, Zan WY, Liu CM, Fu GF, Ma BY, Green synthesis of MgAlON refractories with high strength and excellent slag corrosion resistance. *Ceram. Int.* **2023**, *49*, 37594–37603. DOI:10.1016/j.ceramint.2023.09.086
11. Wang LL, Zhou ZY, Liu CM, Yu C, Deng CJ, Ying ZW, et al. Enhancing the comprehensive performance of MgO–MgAlON composite refractories synthesized from natural minerals. *Ceram. Int.* **2024**, *50*, 30068–30077. DOI:10.1016/j.ceramint.2024.05.305
12. Ma BY, Wang YZ, Zhang W, Chen QY, Pressureless sintering and fabrication of highly transparent MgAlON ceramic from the carbothermal powder. *J. Alloys Compd.* **2018**, *745*, 617–623. DOI:10.1016/j.jallcom.2018.02.254
13. Liu JH, Lv XJ, Li J, Liu YX, Synthesis of molten-electrolyte corrosion resistant $MgAl_2O_4$-MgAlON sidewall materials by pressureless sintering. *J. Alloys Compd.* **2016**, *687*, 623–629. DOI:10.1016/j.jallcom.2016.06.178
14. Chen WB, Wang B, Liu LL, Wang H, WangXD. Preparation and slag erosion resistance mechanism of MgAlON based composite refractories synthesized from solid waste. *Ceram. Int.* **2020**, *46*, 26035–26043. DOI:10.1016/j.ceramint.2020.07.096
15. Zhou J, Li YJ, Duan XH, Chen J, Jin ED, Ding DH, et al. Effects of h-BN on the thermal shock and oxidation resistance of SiO_2-bonded SiC refractories. *Int. J. Appl. Ceram. Technol.* **2024**, *21*, 3526–3537. DOI:10.1111/ijac.14764
16. Zhang ZT, Teng LD, Li WC. Mechanical properties and microstructures of hot-pressed MgAlON–BN composites. *J. Eur. Ceram. Soc.* **2007**, *27*, 319–326. DOI:10.1016/j.jeurceramsoc.2006.04.184
17. Lin H, Feng GQ, Wang HY, Peng HY, Cao LL, Lin HX, et al. Effect of BN addition on mechanical and electrical properties of oxidative sintered porous Si_3N_4-BN composites. *Ceram. Int.* **2023**, *49*, 36637–36645. DOI:10.1016/j.ceramint.2023.08.347
18. Li Q, Yang ZH, Zhong J, Sun YS, Jia DC, Duan XM, et al. Effect of the starting AlN content on the phase formation and property of the novel *in-situ* fabricated X-SiAlON/BN composites. *J. Eur. Ceram. Soc.* **2019**, *39*, 934–943. DOI:10.1016/j.jeurceramsoc.2018.12.035
19. Li M, Zhang LG, Zhang C, Xu EX, Liu XH, Zhao F, et al. Effect of Y_2O_3 on the physical properties and biocompatibility of β–SiAlON ceramics. *Ceram. Int.* **2020**, *46*, 23427–23432. DOI:10.1016/j.ceramint.2020.06.112
20. Abreal A, Goeuriot D, Thevenot F, Lagace M, Gueroult B, Rigaud M. Effect of Y_2O_3 addition on alumina-hex boron nitride composites. *J. Eur. Ceram. Soc.* **1995**, *15*, 841–849. DOI:10.1016/0955-2219(95)00056-Z
21. Podonak MK, Paydar MH, Forghani M, Guo J. B_2O_3 as an effective additive for cold sintering of $MgTiO_3$. *J. Eur. Ceram. Soc.* **2024**, *44*, 261–269. DOI:10.1016/j.jeurceramsoc.2023.08.038
22. Qian F, Li HL, Yang WG, Guo HR, Liu GQ, Li HX, et al. Corrosion resistance of BN–ZrO_2 ceramics with different additives by molten steel. *J. Iron Steel Res. Int.* **2022**, *29*, 1101–1109. DOI:10.1007/s42243-021-00696-x
23. Li YL, Qiao GJ, Jin ZH. Machinable Al_2O_3/BN composite ceramics with strong mechanical properties. *Mater. Res. Bull.* **2002**, *37*, 1401–1409. DOI:10.1016/S0025-5408(02)00786-9
24. Cao RQ, Sun SL, Wang WH, Zan WY, Yuan XZ, Zhou ZY, et al. Preparation and performance optimization of MgO-SiAlON-SiC ceramics using silicon kerf waste. *Ceram. Int.* **2025**, *51*, 39337–39344. DOI:10.1016/j.ceramint.2025.06.171
25. Ren XM, Ma BY, Tian JH, Jiang ZH. The effects of pre-sintering temperature and La_2O_3 addition on sinterability and corrosion resistance of stoichiometric magnesium aluminate spinel. *Ceram. Int.* **2022**, *48*, 32470–32478. DOI:10.1016/j.ceramint.2022.07.193
26. Wang LL, Ma BY, Ren XM, Yu C, Tian JH, Liu CM, et al. Phase-engineering strategy of ZrO_2 for enhancing the mechanical properties of porous cordierite ceramics. *Mater. Today Commun.* **2022**, *30*, 103032. DOI:10.1016/j.mtcomm.2021.103032
27. Xu YH, Ji ZX, Yang ZY, Yang JS, Li R, Fu ZD, et al. Densification and comprehensive properties of h-BN-based refractories with *in-situ* formation of $Y_3Al_5O_{12}$. *J. Alloys Compd.* **2021**, *875*, 160018. DOI:10.1016/j.jallcom.2021.160018
28. Sun Y, Chen YS, Tian L, Li GH, Formation mechanism of MgAlON phase in aluminum–magnesia composite materials. *Mater. Chem. Phys*. **2017**, *197*, 65–69. DOI:10.1016/j.matchemphys.2017.05.008
29. Zhai FR, Li S, Sun JL, Yi ZZ. Microstructure, mechanical properties and thermal shock behavior of h-BN-SiC ceramic composites prepared by spark plasma sintering. *Ceram. Int.* **2017**, *43*, 2413–2417. DOI:10.1016/j.ceramint.2016.11.030
30. Ma BY, Tang YD, Deng CJ. Effects of Al_2O_3–Y_2O_3/Yb_2O_3 additives on microstructures and mechanical properties of silicon nitride ceramics prepared by hot-pressing sintering. *Int. J. Appl. Ceram. Technol.* **2022**, *19*, 2523–2532. DOI:10.1111/ijac.14081

31. Ren XM, Ma BY, Tang JH, Li YW, Yu JK. Fabrication of energy-saving MgO with large grain size and low thermal conductivity: Towards a new type of magnesia for high-temperature furnaces. *Constr. Build. Mater.* **2022**, *342*, 128097. DOI:10.1016/j.conbuildmat.2022.128097
32. Shi JL, Deguchi Y, Sakabe Y. Relation between grain growth, densification and surface diffusion in solid state sintering—A direct observation. *J. Mater. Sci.* **2005**, *40*, 5711–5719. DOI:10.1007/s10853-005-1474-7
33. Ren XM, Ma BY, Liu H, Wang ZF, Deng CJ, Liu GQ, et al. Designing low-carbon MgO–Al_2O_3–La_2O_3–C refractories with balanced performance for ladle furnaces. *J. Eur. Ceram. Soc.* **2022**, *42*, 3986–3995. DOI:10.1016/j.jeurceramsoc.2022.03.051
34. Zhang ZT, Seetharaman S, Li WC. Thermal diffusivity/conductivity of MgAlON-BN composites. *Metall. Mater. Trans. B* **2006**, *37*, 615–621. DOI:10.1007/s11663-006-0045-4
35. Evans AG, Faber KT. Toughening of ceramics by circumferential microcracking. *J. Am. Ceram. Soc.* **1981**, *64*, 394–398. DOI:10.1111/j.1151-2916.1981.tb09877.x
36. Retajczyk TF, Sinha AK. Elastic stiffness and thermal expansion coefficient of BN films. *Appl. Phys. Lett.* **1980**, *36*, 161–163. DOI:10.1063/1.91415
37. Wang ZJ, Alaniz JE, Jang WY, Garay JE, Dames C. Thermal conductivity of nanocrystalline silicon: Importance of grain size and frequency-dependent mean free paths. *Nano Lett.* **2011**, *11*, 2206–2213. DOI:10.1021/nl1045395
38. Schramm A, Nowak R, Bruzda G, Polkowski W, Fabrichnaya O, Aneziris CG. High temperature wettability and corrosion of ZrO_2, Al_2O_3, Al_2O_3-C, MgO and MgAlON ceramic substrates by an AZ91 magnesium alloy melt. *J. Eur. Ceram. Soc.* **2022**, *42*, 3023–3035. DOI:10.1016/j.jeurceramsoc.2022.01.040
39. Liu JH, Sheng HY, Yang X, He ZJ, Hou XM. Research on the wetting and corrosion behavior between converter slag with different alkalinity and MgO-C refractories. *Oxid. Met.* **2022**, *97*, 157–166. DOI:10.1007/s11085-021-10083-2